THE ASTROPHYSICAL JOURNAL, 441:18–27, 1995 March 1

RADIATIVE TRANSFER IN A CLUMPY UNIVERSE: THE COLORS OF HIGH-REDSHIFT GALAXIES

PIERO MADAU
Space Telescope Science Institute, 3700 San Martin Drive, Baltimore, MD 21218
Received 1993 December 3; accepted 1994 September 9

ABSTRACT

We assess the effects of the stochastic attenuation produced by intervening QSO absorption systems on the broadband colors of galaxies at cosmological distances. We compute the H I opacity of a clumpy universe as a function of redshift, including scattering in resonant lines, such as Lyα, Lyβ, Lyγ, and higher order members, and Lyman-continuum absorption. Both the numerous, optically thin Lyman-α forest clouds and the rarer, optically thick Lyman limit systems are found to contribute to the obscuration of background sources. We study the mean properties of primeval galaxies at high redshift in four broad optical passbands, U_n, B, G, and $\mathscr{R}$. Even if young galaxies radiated a significant amount of ionizing photons, the attenuation due to the accumulated photoelectric opacity along the path is so severe that sources beyond $z \sim 3$ will drop out of the U_n image altogether. We also show that the observed $B-\mathscr{R}$ color of distant galaxies can be much redder than expected from a stellar population. At $z \sim 3.5$, the blanketing by discrete absorption lines in the Lyman series is so effective that background galaxies appear, on average, 1 mag fainter in B. By $z \sim 4$, the observed B magnitude increment due to intergalactic absorption exceeds 2 mag. By modeling the intrinsic UV spectral energy distribution of star-forming galaxies with a stellar population synthesis code, we show that the $(B-\mathscr{R})_{AB} \sim 0$ criterion for identifying "flat-spectrum," metal-producing galaxies is biased against objects at $z > 3$. The continuum blanketing from the Lyman series produces a characteristic staircase profile in the transmitted power. We suggest that this cosmic Lyman decrement might be used as a tool to identify high-z galaxies.

Subject headings: cosmology: observations — galaxies: evolution — intergalactic medium — quasars: absorption lines — radiative transfer — ultraviolet: galaxies

1. INTRODUCTION

Absorption by intervening material can seriously distort our view of objects at cosmological distances. Although some of the obscuring gas might be uniformly distributed in the intergalactic space, the plethora of absorption lines seen in the spectra of background quasars indicates that much absorbing material is located in discrete systems. Enough neutral hydrogen and singly ionized helium is contained in the intergalactic clumps of highly ionized primordial gas which form the Lyman-α forest, and in the metal-line absorption systems associated with the halo regions of bright galaxies, to significantly attenuate the ionizing flux from distant sources (Bechtold et al. 1987; Miralda-Escudé & Ostriker 1990; Møller & Jakobsen 1990; Madau 1991, 1992; Meiksin & Madau 1993; Zuo & Phinney 1993). Hydrogen absorption along the line of sight is known to affect the path of quasars in color space as a function of redshift (Giallongo & Trevese 1990). The extinction produced by dust grains within the damped Lyman-α systems—the likely progenitors of galactic disks—may redden and obscure background quasars (Fall & Pei 1993). It is the purpose of this paper to construct a detailed model of the H I opacity of the universe and to examine the effects of various absorption mechanisms on the broadband colors of cosmological distant galaxies.

In the past few years, much observing time has been devoted to the problem of the detection of galaxies at high redshift (for a recent review of the searches for primeval galaxies, see Djorgovski & Thompson 1992). It is anticipated that any knowledge of their early luminosity and color evolution will put constraints on the history of structure formation. Deep CCD imaging surveys down to $B \sim 27$ have revealed a high surface density of weakly clustered, faint blue galaxies (Tyson 1988; Guhathakurta, Tyson, & Majewski 1990; Lilly, Cowie, & Gardner 1991). While the bulk of the $B < 24$ population is represented by "normal" dwarfs at $z \lesssim 0.4$, the nature of the faintest, $B > 24$ objects remains unclear. A small fraction of these galaxies have truly flat spectral energy distributions (Lilly et al. 1991). The blue, $(B-I)_{AB} \sim 0$ colors might be the signature of a population of young objects undergoing a burst of star formation, with high-mass stars producing metals and UV photons which are redshifted into the blue band.

Despite a large amount of efforts, observations of the colors and luminosities of the highest redshift galaxies have been limited to a handful of very bright, likely unrepresentative, radio-loud objects (Chambers, Miley, & Van Breugel 1990). A list of primeval galaxy candidates has been recently presented by Steidel & Hamilton (1992, 1993), as a result of a new "ultradeep" imaging survey of the fields of high-z QSOs which exhibit intervening optically thick absorption systems in the redshift range $3 < z_{abs} < 3.5$. A custom filter set is chosen (three optical passbands called U_n, G, and $\mathscr{R}$) to provide the maximum color information. Narrow-band imaging and spectroscopic surveys have also made use of QSO absorption-line systems to flag possible locations of high-redshift galaxies (Lowenthal et al. 1991; Macchetto et al. 1993). The nature of these objects is crucial to our understanding of galaxy evolution. Key questions to be answered are as follows: How can we identify high-redshift galaxies in CCD surveys? Are they forming stars more rapidly than typical quiescent spiral galaxies at the present epoch? Are they obscured by dust in analogy with the luminous *IRAS* starbursts at low redshifts? Can their colors be related to theoretical synthetic spectra?

There exist two complementary aspects of intergalactic obscuration which we want to explore here. First, intervening absorbing material will hamper the evaluation of the intrinsic, far-UV photometric properties of galaxies at high z. As hydrogen Lyα enters the B and G passbands at $z_{em} \sim 2.5$, the blanketing by discrete absorption lines causes a significant depression in the source broadband continuum intensity shortward of 1216 Å in the emitter rest frame. At $z \sim 2.7$, the Lyman break moves into the U band, and the attenuation due to the accumulated photoelectric absorption by optically thin and thick systems along the line of sight produces a large reduction of the ionizing flux. The observed $U_n - G$ (or, equivalently, $U - B$) and $G - \mathcal{R}(B - R)$ colors of galaxies at $z \gtrsim 3$ can then appear much redder than expected from a young stellar population (cf. Steidel & Hamilton 1992; Guhathakurta et al. 1990; Bithell 1991). Second, neutral hydrogen along the path will, at the same time, produce distinctive absorption features in the spectra of background UV sources. At low resolution, discontinuities in the cosmic transmission appear at characteristic frequencies, which, we shall argue, can be used as a tool to identify high-z objects. The plan of the paper is a follows. In § 2 we analyze the statistical properties of the absorption of photons in a clumpy universe and present our detailed model. We consider the attenuation of background sources by Lyman-α forest clouds and metal-line systems in the foreground, including scattering in resonant lines, such as Lyα, Lyβ, Lyγ, and higher order members, and continuum absorption (Møller & Jakobsen 1990). In § 3 we discuss the "reddening" effect that these atomic processes produce on the observed broadband colors of cosmological distant galaxies. We summarize our results in § 4 and address some possible strategies for recognizing star-forming galaxies at high redshift.

2. THE STATISTICS OF INTERVENING ABSORPTION

2.1. *Basic Theory*

A full analysis of the statistical properties of any attenuation caused by Poisson-distributed absorbers along the line of sight requires the knowledge of the probability density for the total optical depth along the path (Wright 1986; Ostriker & Heisler 1984). In the following, we shall assume Poisson-distributed absorbers, neglecting the clustering effects observed, e.g., in the C IV–selected systems (Sargent, Boksenberg, & Steidel 1988). If we define $\rho(\tau_c, z)d\tau_c\, dz$ as the mean number of absorbers along the line of sight in the redshift interval $(z, z + dz)$, each having optical depth in the range $(\tau_c, \tau_c + d\tau_c)$, the probability $p(\tau \mid z)$ that the total optical depth in a random direction to a redshift z lies in the interval $(\tau, \tau + d\tau)$ is (Fall & Pei 1989)

$$p(\tau \mid z) = \int_{-\infty}^{+\infty} \exp\left\{-2\pi i s\tau + \int_0^z [\tilde{\rho}(s, z') - \tilde{\rho}(0, z')]dz'\right\} ds\,, \tag{1}$$

where

$$\tilde{\rho}(s, z') = \int_0^{\infty} \rho(\tau_c, z') \exp(2\pi i s\tau_c) d\tau_c \tag{2}$$

is the Fourier transform on the variable τ_c, and all optical depths are measured at a fixed wavelength in the rest frame of the observer. The probability function contains all statistical information about the attenuation in a random line of sight. Let $L(\nu_{em})$ be the specific power emitted with frequency ν_{em} by a source at redshift z_{em}. The mean specific flux observed at Earth is

$$\langle f(\nu_{obs})\rangle = \frac{(1 + z_{em})L(\nu_{em})}{4\pi d_L^2(z_{em})} \langle e^{-\tau}\rangle\,, \tag{3}$$

where $\nu_{obs} = \nu_{em}/(1 + z_{em})$, $d_L(z_{em})$ is the luminosity distance, and the average transmission over all lines of sight is

$$\langle e^{-\tau}\rangle = \int e^{-\tau} p(\tau) d\tau = \exp\left[\int_0^{z_{em}} \int \frac{\partial^2 N}{\partial N_{H\,I}\,\partial z} (1 - e^{-\tau_c}) dN_{H\,I}\, dz\right], \tag{4}$$

where τ_c is the optical depth through an individual cloud at frequency $\nu = \nu_{obs}(1 + z)$, and $\rho(\tau_c, z) = (\partial^2 N/\partial N_{H\,I}\,\partial z)(\partial \tau_c/\partial N_{H\,I})^{-1}$. The *effective* optical depth of a cloudy medium can then be defined as $\tau_{eff} = -\ln(\langle e^{-\tau}\rangle)$ (Paresce, McKee, & Bowyer 1980). When $\tau_c \ll 1$, τ_{eff} becomes equal to the mean optical depth. In the opposite limit, the obscuration is picket fence–type, and the effective optical depth becomes equal to the mean number of optically thick systems along the line of sight.[1] A measure of the expected scatter around $\langle e^{-\tau}\rangle$ due to statistical fluctuations in the number of absorbing clouds along the line of sight is given by (Møller & Jakobsen 1990)

$$\sigma^2(e^{-\tau}) = \int (e^{-\tau} - \langle e^{-\tau}\rangle)^2 p(\tau) d\tau = \exp\left[-\int_0^{z_{em}} \int \frac{\partial^2 N}{\partial N_{H\,I}\,\partial z} (1 - e^{-2\tau_c}) dN_{H\,I}\, dz\right] - e^{-2\tau_{eff}}\,. \tag{5}$$

We can use convolution integrals to study the effects of intervening Lyman-α forest clouds and metal systems on the propagation of far-UV radiation. If we denote with $p_1(\tau)$ and $p_2(\tau)$ the probability densities produced by such two distinct populations of absorbers, the total optical depth distribution $p(\tau)$ can be expressed as the convolution of the individual distributions:

$$p(\tau) = \int_0^{\tau} p_1(x) p_2(\tau - x) dx\,, \tag{6}$$

with the total effective opacity being the sum of the individual effective depths, $\tau_{eff} = \tau_{eff,1} + \tau_{eff,2}$. We can also apply the convolution theorem when the absorption cross section is a narrow, strongly peaked function, as in the case of resonant scattering

[1] To shed some light on the adopted formalism, it is instructive to consider the situation in which all absorbers have the same optical depth τ_0 independent of redshift, and the mean number of systems along the path is $\Delta N = \int dz\, dN/dz$. In this case we have $\rho(\tau_c) = \delta(\tau_c - \tau_0) dN/dz$, $\tilde{\rho}(s) = e^{2\pi i s\tau_0} dN/dz$, $\tilde{p}(s) = \exp[\Delta N(e^{2\pi i s\tau_0} - 1)]$, and $\langle e^{-\tau}\rangle = \exp[-\Delta N(1 - e^{-\tau_0})]$, where $\delta(x)$ denotes the usual delta function. Integrating eq. (1) by the residue theorem we recover the simple Poisson formula for the probability of encountering a total optical depth $k\tau_0$ along the line of sight (with k integer), $p(k\tau_0) = e^{-\Delta N} \Delta N^k/(\tau_0\, k!)$. The mean optical depth is, trivially, $\langle\tau\rangle = \Delta N \tau_0$, and always exceeds $\tau_{eff} = \Delta N(1 - e^{-\tau_0})$.

in the lines of the Lyman series. As different atomic lines dominate the cosmic opacity at different absorption redshifts, the total optical depth in a random direction at a fixed observed wavelength can be written as the sum of independent random variables.

2.2. *The Distribution in Column Density and Redshift of the Absorbers*

Since the bluest optical filter we are interested in is the U_n bandpass (effective wavelength ~ 3500 Å), our background sources will only be subject to H I absorption from material located at $z \gtrsim 1.9$. The numerous, optically thin clouds which form the Lyman-α forest are intergalactic objects which evolve rapidly between $1.8 < z < 3.8$ (Murdoch et al. 1986) and are not associated with heavy elements. The distribution of the rarer optically thick Lyman limit systems is instead consistent with no evolution over the range $0.7 < z < 3.6$ (Sargent, Steidel, & Boksenberg 1989). About $\frac{2}{3}$ of the Lyman limit absorbers are associated with heavy element lines.

The distribution of line rest equivalent widths for the Lyman-α forest is known to follow an exponential for $W > 0.2$ Å,

$$\frac{\partial^2 N}{\partial W\, \partial z} = \frac{N_0}{W_*}\, e^{-W/W_*}(1+z)^{\gamma}\,, \tag{7}$$

where $W_* = 0.3$ Å (Murdoch et al. 1986). Following Press & Rybicki (1993), we take $\gamma = 2.46$ and $N_0 = 12.2$. For $W < 0.2$ Å, the number of lines shows a sharp rise (Murdoch et al. 1986), which is well fitted by a power-law distribution,

$$\frac{\partial^2 N}{\partial W\, \partial z} = \frac{3.4}{W_*}\left(\frac{W}{W_*}\right)^{-\beta}(1+z)^{2.46}\,, \tag{8}$$

where $\beta = 1.5$ and we have assumed that these weak lines also evolve as $(1+z)^{2.46}$.

The equivalent width distribution of Lyα lines associated with metal-containing systems is only poorly determined. The data suggest an exponential form with an e-folding width $W_* = 1.6$ Å (Tytler 1987). We use the Lyman limit systems as a tracer of the heavy element absorbers (e.g., Steidel 1990), and normalize following Sargent et al. (1989) to obtain

$$\frac{\partial^2 N}{\partial W\, \partial z} = \frac{1.3}{W_*}\, e^{-W/W_*}(1+z)^{0.68}\,. \tag{9}$$

There is some overlap in H I column density between Lyα only and metal-line systems. Tytler (1987) found that both populations coexist in the range $0.5 < W < 2$ Å.

We may use a standard curve of growth analysis to self-consistently derive the H I column density distribution of the Lyman-α forest clouds. If we assume, for simplicity, that the Doppler parameter is the same for all clouds, $b = 35$ km s^{-1} (close to the mean value derived by Rauch et al. 1992), then a power-law $dN/dN_{\rm H\,I} \propto N_{\rm H\,I}^{-\beta}$ is found to be a good approximation, with a slope $\beta = 1.56$ for $2 \times 10^{12} < N_{\rm H\,I} < 5 \times 10^{14}$ cm^{-2}, and $\beta = 1.29$ for $5 \times 10^{14} < N_{\rm H\,I} < 10^{17}$ cm^{-2}. Previous determinations based on line fitting and counting typically yield a value in the range 1.5–1.8 (Tytler 1987; Carswell et al. 1991; Rauch et al. 1992). To facilitate a comparison with previous studies (Miralda-Escudé & Ostriker 1990; Madau 1991, 1992), we shall assume in the following a constant value of $\beta = 1.5$ as $N_{\rm H\,I}$ varies from 2×10^{12} to 10^{20} cm^{-2} (Tytler 1987; Sargent et al. 1989). We take

$$\frac{\partial^2 N}{\partial N_{\rm H\,I}\, \partial z} = \begin{cases} 2.4 \times 10^{7} N_{\rm H\,I}^{-1.5}(1+z)^{2.46} & (2 \times 10^{12} < N_{\rm H\,I} < 1.59 \times 10^{17}\ {\rm cm}^{-2})\,; \\ 1.9 \times 10^{8} N_{\rm H\,I}^{-1.5}(1+z)^{0.68} & (1.59 \times 10^{17} < N_{\rm H\,I} < 10^{20}\ {\rm cm}^{-2})\,. \end{cases} \tag{10}$$

This model is broadly consistent with the determinations mentioned above and provides about the same photoelectric opacity as in model A2 of Miralda-Escudé & Ostriker (1990), and in the medium attenuation model MA of Meiksin & Madau (1993). However, it is fair to point out that there is very limited information on Lyman-α forest absorbers with $10^{16} \lesssim N_{\rm H\,I} \lesssim 10^{17}$ cm^{-2}. As $\beta < 2$, these high column density clouds will dominate the Lyman-α forest contribution to the effective photoelectric optical depth, making its value rather uncertain.[2]

2.3. Lyα *Line Blanketing*

At wavelengths shortward of Lyα in the emitter rest frame, the source's continuum intensity is attenuated by the combined blanketing effect of many absorption lines. Let us consider Lyα resonant scattering first. As the wavelengths of photons at observation, absorption, and emission are related by $\lambda_{\rm obs} = (1+z_{\rm abs})\lambda_{\rm abs} = (1+z_{\rm em})\lambda_{\rm em}$, and since the optical depth of a cloud located at the absorption redshift $z_{\rm abs}$ has a narrow peak at $\lambda_{\rm obs} = \lambda_\alpha(1+z_{\rm abs})$, we derive

$$\tau_{\rm eff} = \frac{\lambda_{\rm obs}}{\lambda_\alpha^2}\int \frac{\partial^2 N}{\partial W\, \partial z}\, W\, dW\,, \tag{11}$$

for $\lambda_\beta(1+z_{\rm em}) < \lambda_{\rm obs} < \lambda_\alpha(1+z_{\rm em})$, where $\lambda_\alpha = 1216$ Å and $\lambda_\beta = 1026$ Å. Here, the distribution $\partial^2 N/\partial W\, \partial z$ is computed at $z_{\rm obs} = \lambda_{\rm obs}/\lambda_\alpha - 1$. Using equations (7) and (8), and integrating from 0.01 to 2 Å, we obtain for the Lyman-α forest contribution

$$\tau_{\rm eff} = 0.0036\left(\frac{\lambda_{\rm obs}}{\lambda_\alpha}\right)^{3.46}\,, \tag{12}$$

in agreement with the results of Press, Rybicki, & Schneider (1993). Saturated lines with $W \geq 0.5$ Å contribute $\sim 40\%$ to $\tau_{\rm eff}$. From equation (9), and integrating from $W = 0.5$ Å to infinity, we derive for metal lines

$$\tau_{\rm eff} = 0.0017\left(\frac{\lambda_{\rm obs}}{\lambda_\alpha}\right)^{1.68}\,. \tag{13}$$

[2] Meiksin & Madau (1993) have recently suggested that the published data may indicate a significant underdensity of Lyman-α clouds with columns $N_{\rm H\,I} > 10^{15}$ cm^{-2}. This deficit, if real, would result in a reduction of the forest photoelectric opacity relative to the adopted model.

Although the relative importance of metal systems increases for the higher order Lyman series lines, we have checked that heavy element absorbers make a negligible contribution to the line blanketing effective cosmic opacity in the range $2.5 \lesssim z \lesssim 4.5$ of interest in this study. For simplicity, we will neglect them in the following and take equation (12) as our best estimate of the effective optical depth produced by Lyα resonant scattering from intervening material.

An analytical expression for the probability distribution can also be obtained. As the optical depth at the line center is large, about $2.2 \times 10^{-14} N_{\rm H\,I}(b/35 \text{ km s}^{-1})^{-1}$, it is a good approximation to extend the integration over τ_c in equation (2) from 0 to infinity. A close form for $p(\tau)$ can then be derived in the special case of $\beta = 1.5$ (Zuo & Phinney 1993),

$$p(\tau) = \frac{\tau_{\rm eff}}{2\sqrt{\pi}} \exp\left(-\frac{\tau_{\rm eff}^2}{4\tau}\right)\tau^{-3/2} . \tag{14}$$

The cumulative probability is $P(>\tau) = \text{erf}\,(0.5\tau_{\rm eff}/\tau^{1/2})$, where erf (x) is the error function.

2.4. *Lyman Series Line Blanketing*

When $\lambda_{\rm obs} \leq \lambda_\beta(1 + z_{\rm em})$, a significant contribution to the blanketing opacity comes from the higher order lines of the Lyman series. We have applied a standard curve-of-growth analysis, assuming $b = 35$ km s^{-1} for all clouds, to numerically compute the attenuation expected from line blanketing of Lyβ, Lyγ, Lyδ, plus 13 higher order members. In the wavelength range $\lambda_{i+1}(1 + z_{\rm em}) < \lambda_{\rm obs} < \lambda_i(1 + z_{\rm em})$, the total effective line-blanketing optical depth can be written as the sum of the contributions from the $j \rightarrow 1$ transitions,

$$\tau_{\rm eff} = \sum_{j=2,i} A_j \left(\frac{\lambda_{\rm obs}}{\lambda_j}\right)^{3.46} , \tag{15}$$

where $A_j = (1.7 \times 10^{-3}, 1.2 \times 10^{-3}, 9.3 \times 10^{-4})$, and $\lambda_j = (1026, 973, 950$ Å) for Lyβ, Lyγ, and Lyδ, respectively. These estimates are weakly sensitive to the assumed velocity width. We have checked that a (constant) value of $b = 45$ km s^{-1} would decrease the coefficients A_3, A_4, and A_5 by 12%, 20%, and 25%, respectively. The absorption strengths of Lyβ, Lyγ, and Lyδ relative to Lyα, $A_3/A_2 = 0.47$, $A_4/A_2 = 0.33$, and $A_5/A_2 = 0.26$, where $A_2 = 3.6 \times 10^{-3}$ from equation (12), are consistent with the values derived by Press et al. (1993) from the Schneider, Schmidt, & Gunn (1991a) sample of $z > 3$ QSOs.

In Figure 1*a* we plot the distribution $p(\tau)$ as a function of the Lyα line-blanketing optical depth for photons observed at $\lambda_{\rm obs} = \lambda_\alpha(1 + z_{\rm em})$, and of the cumulative Lyα, Lyβ, Lyγ, and Lyδ opacity at $\lambda_{\rm obs} = \lambda_\delta(1 + z_{\rm em})$, with $z_{\rm em} = 3.5$.

2.5. *Photoelectric Absorption by Intervening Systems*

Continuum absorption from neutral hydrogen along the line of sight affects photons observed at $\lambda_{\rm obs} < \lambda_{\rm L}(1 + z_{\rm em})$, where $\lambda_{\rm L} = 912$ Å is the Lyman limit. The effective photoelectric optical depth of Poisson-distributed systems is

$$\tau_{\rm eff} = \int_{z_c}^{z_{\rm em}} \int_{N_{\rm H\,I,\,min}}^{N_{\rm H\,I,\,max}} \frac{\partial^2 N}{\partial N_{\rm H\,I}\,\partial z}(1 - e^{-N_{\rm H\,I}\sigma}) dN_{\rm H\,I}\, dz , \tag{16}$$

where $\sigma(\lambda_{\rm obs}, z) = 6.3 \times 10^{-18}(\lambda_{\rm obs}/\lambda_{\rm L})^3(1 + z)^{-3}$ cm^2 is the hydrogen photoionization cross section, and $(1 + z_c) = (\lambda_{\rm obs}/\lambda_{\rm L})$ for $\lambda_{\rm obs} > \lambda_{\rm L}$ (when $\lambda_{\rm obs} \leq \lambda_{\rm L}$, H I absorbs photons all the way down to $z_c = 0$).[3] Note that the He I contribution to the attenuation is negligible in the case of a QSO-dominated ionizing background, while He II absorption on the way must be included if $(1 + z_{\rm em}) > \lambda_{\rm obs}/228$ Å.

The complicated, two-population form of the column density distribution in equation (10) precludes the use of the analytical expression given in equation (14) for a statistical study of cosmological photoelectric absorption. One must therefore first calculate numerically the Fourier transform of the function $\rho(\tau_c)$, and then apply a fast Fourier transform technique to get the probability density $p(\tau)$. Figure 1*b* depicts $p(\tau)$ as a function of the continuum opacity alone. The optical depth is measured at $\lambda_{\rm obs} = 3570$ Å, the effective wavelength of Steidel & Hamilton's ultraviolet bandpass, along a random line of sight to $z_{\rm em} = 3.5$. We find that, as expected, the most likely values of τ are much less than the mean as the distribution is highly skewed due to the presence of Lyman limit systems. By contrast, because of the large number of optically thin absorbers, the probability function for the Lyman-α forest alone is not too far from Gaussian (central limit theorem).

2.6. *Comparison with the Observed D_A and D_B*

In modeling intergalactic absorption, we have assumed that the observed equivalent width distribution of the Lyman-α forest clouds is a true representation of the actual one, with line blending not severely affecting its determination over the relevant redshift range. We can actually test the validity of our estimated strength and overall trend with redshift of the absorption accumulated along a random path by examining some simple properties of the quasar fluxes below their Lyα emission feature, namely the observed flux deficits D_A and D_B (Oke & Korycansky 1982; Schneider et al. 1991a). We compute the mean (over all lines of sight) wavelength-averaged attenuation of the quasar's continuum due to line blanketing as

$$\langle D_A \rangle = 1 - \frac{1}{\Delta\lambda_A} \int_{1050(1+z_{\rm em})}^{1170(1+z_{\rm em})} \exp\left[-A_2\left(\frac{\lambda_{\rm obs}}{\lambda_\alpha}\right)^{3.46}\right] d\lambda_{\rm obs} , \tag{17}$$

[3] An approximate (within 5%) integration of eq. (16) yields $\tau_{\rm eff} \simeq 0.25x_c^3(x_{\rm em}^{0.46} - x_c^{0.46}) + 9.4x_c^{1.5}(x_{\rm em}^{0.18} - x_c^{0.18}) - 0.7x_c^3(x_c^{-1.32} - x_{\rm em}^{-1.32}) - 0.023(x_{\rm em}^{1.68} - x_c^{1.68})$, where $x_c \equiv 1 + x_c$, and $x_{\rm em} \equiv 1 + z_{\rm em}$. The first term on the right-hand side represents the approximate contribution of Lyman-α clouds; the others are due to Lyman limit systems.

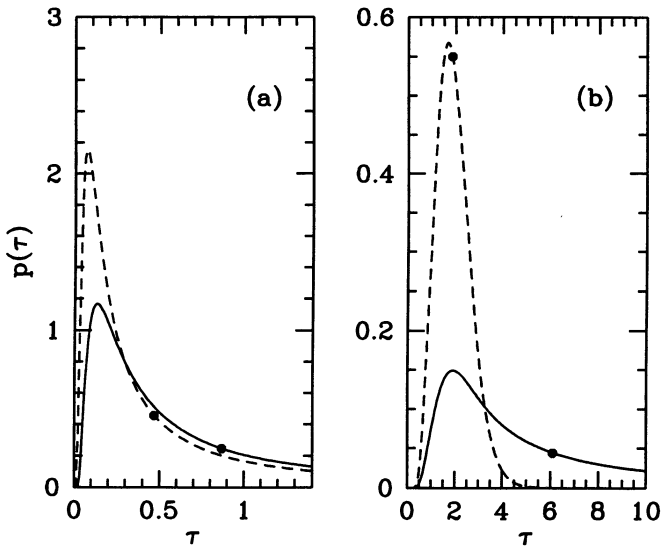

FIG. 1.—Probability density for the total optical depth τ in a random direction to a redshift $z_{em} = 3.5$. A dot on each curve indicates the median point where the integral over τ equals 0.5. (*a*) Distribution functions for the Lyα line blanketing opacity at $\lambda_{obs} = 1216(1 + z_{em})$ Å (*dashed line*), and for the Lyα, Lyβ, Lyγ, and Lyδ line opacity at $\lambda_{obs} = 950(1 + z_{em})$ Å (*solid line*). (*b*) Distribution function for the accumulated photoelectric optical depth at $\lambda_{obs} = 3570$ Å. *Solid line*: Lyman-α forest plus Lyman limit system total continuum opacity. *Dashed line*: probability function for the Lyman-α forest alone.

where $\Delta\lambda_A = 120(1 + z_{em})$ Å, and

$$\langle D_B \rangle = 1 - \frac{1}{\Delta\lambda_B} \int_{920(1+z_{em})}^{1015(1+z_{em})} \exp\left[- \sum_{j=3,11} A_j \left(\frac{\lambda_{obs}}{\lambda_j} \right)^{3.46} \right] d\lambda_{obs} , \tag{18}$$

where $\Delta\lambda_B = 95(1 + z_{em})$ Å. Our determination of the contribution to $\langle D_A \rangle$ and $\langle D_B \rangle$ from the Lyman-α forest is shown in Figure 2. Overall, the absorption model adopted here fits rather well the measurements of Steidel & Sargent (1987), Giallongo & Cristiani

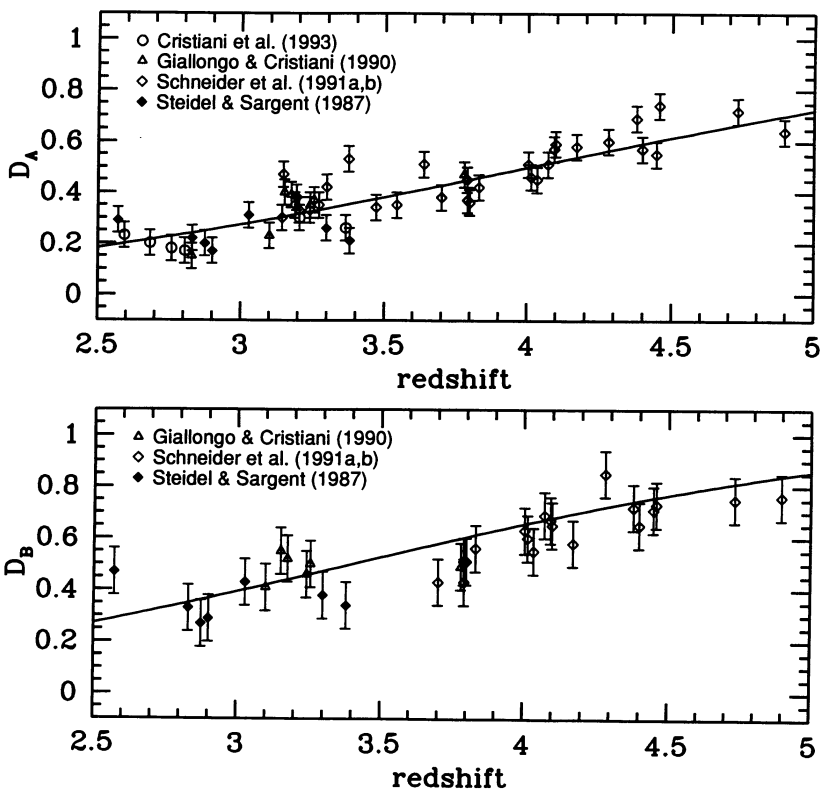

FIG. 2.—The measured QSO flux decrements D_A and D_B as a function of redshift. The four broad absorption line quasars PC 2048+0126, PC 2330+0125, Q0051−279, and Q0903+1734 have been eliminated from the sample. The solid line is the estimated mean contribution from the Lyman-α forest. The (constant) vertical error bars are from Schneider et al. (1991a), who assign a 1 σ uncertainty of ± 0.05 and ± 0.09 to their measurements of D_A and D_B, respectively.

(1990), Schneider et al. (1991a, b), and Cristiani et al. (1993) in the redshift range $2.5 < z < 5$. A distribution of Doppler parameters might improve the overall fit. Notice that Steidel & Sargent have argued that there might be a tendency to overestimate the continuum in lower resolution data, thus overestimating the measured D_A.

3. IMPLICATIONS

3.1. *Mean Transmission of the Universe*

Photons emitted at redshift z_{em} and observed at wavelength $\lambda_{obs} < 912(1 + z_{em})$ Å suffer Lyman series line blanketing from absorbers located at redshifts $\lambda_{obs}/\lambda_\alpha - 1$, $\lambda_{obs}/\lambda_\beta - 1$, $\lambda_{obs}/\lambda_\gamma - 1$, etc., and photoelectric absorption from material at $z_{abs} > \lambda_{obs}/\lambda_L - 1$. As the line blanketing and continuum optical depths are independent random variables, the probability functions for the total opacity along a random direction is given by the convolution of the individual distributions. Figure 3*a* shows the characteristic staircase profile of the mean cosmic transmission $\langle e^{-\tau} \rangle$ for a source at $z_{em} = 3.5$ as a function of observed wavelength, together with the expected ± 1 σ rms scatter caused by statistical fluctuations in the absorbers' line-of-sight number density. Largely due to a higher normalization for the density of absorbers at high redshift, our model of intergalactic absorption produces a mean attenuation which is larger than Møller & Jakobsen (1990) Monte Carlo calculations. Figure 3*b* displays the transmission spectrum for a source at $z_{em} = 2.5$, 3.5, and 4.5, averaged over all paths. The dependence with redshift is fairly steep. Just shortward of Lyα in the emitter rest-frame, $\langle e^{-\tau} \rangle$ ranges from 0.76 ± 0.31 at $z_{em} = 2.5$ to 0.27 ± 0.29 at $z_{em} = 4.5$. In the same redshift interval, but just longward of the Lyman limit, $\lambda_{obs} \gtrsim \lambda_L(1 + z_{em})$, $\langle e^{-\tau} \rangle$ ranges from 0.46 ± 0.34 to 0.023 ± 0.066.

Also plotted in Figure 3*b* are the response functions of the photometric system we shall adopt in our discussion. This consists of a standard Johnson *B* filter and the three broad passbands U_n, *G*, and $\mathcal{R}$ used by Steidel & Hamilton (1992, 1993) in their deep CCD imaging survey. The U_n filter has a red-side cutoff which is ~ 100 Å bluer than the standard *U*, while the $\mathcal{R}$ bandpass response is placed in wavelength between *R* and *I*. The U_n, *G*, and $\mathcal{R}$ passbands have similar effective wavelengths to the *U*, B_J, and *R* filters used by Guhathakurta et al. (1990). By design, the U_n and *G* passbands are optimally placed to straddle the Lyman-continuum break of a galaxy at $3 \lesssim z_{em} \lesssim 3.5$. It is clear that the observed broadband colors of cosmological distant objects will be strongly "reddened" by continuum absorption and blanketing of discrete absorption lines which move into and out of the color passbands with changing *z*. To be quantitative, we must take into account that the mean transmission observed is not $\langle e^{-\tau} \rangle$ but rather an average over the bandpass,

$$Q(z_{em}) = \int e^{-\tau_{eff}} T(\lambda) d\lambda \,, \tag{19}$$

where $T(\lambda)$ is the normalized transmittance of the relevant filter. It is useful to measure the mean integrated attenuation in magnitudes, $\Delta m = -1.086 \ln Q$. Figure 4 shows ΔU_n, ΔB, and ΔG, the observed magnitude increases at the corresponding bandpass due to intervening absorption, as a function of emission redshift. These increments must be added to the term $-1.086 \ln(1 + z_{em})$ to

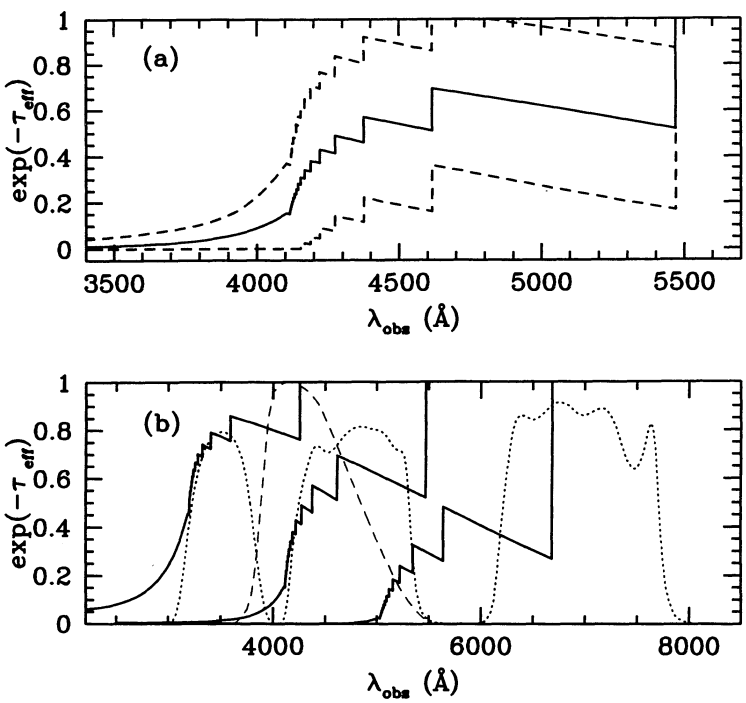

FIG. 3.—Transmission of the universe as a function of observed wavelength, averaged over all lines of sight. (*a*) Mean cosmic transmission for a source at $z_{em} = 3.5$ (*solid line*), together with the expected ± 1 σ rms scatter caused by statistical fluctuations in the number of absorbers along the path (*dashed lines*). The characteristic staircase profile is due to continuum blanketing from the Lyman series. (*b*) Mean transmission spectrum for a source at $z_{em} = 2.5$, 3.5, and 4.5 (*solid lines*). Also plotted are the response functions of a standard Johnson *B* filter (*dashed line*), and the three broad passbands, U_n, *G*, and $\mathcal{R}$ used by Steidel & Hamilton (*dotted lines*).

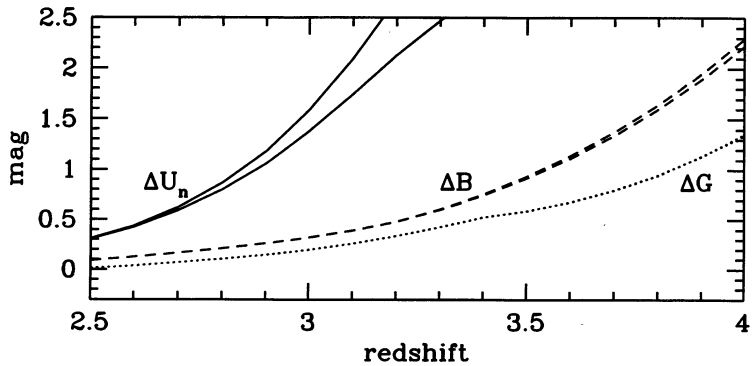

FIG. 4.—Magnitude increments ΔU_n (*solid lines*), ΔB (*dashed lines*), and ΔG (*dotted line*), derived by integrating the mean cosmic transmission over the corresponding bandpass, as a function of the emission redshift. The lowest of each pair of curves includes photoelectric absorption by Lyman-α clouds alone.

get the standard K-correction for a flat emitted spectrum. As H I absorption will not affect the $\mathscr{R}$ passband for $z_{em} \lesssim 4.5$, $\Delta\mathscr{R} = 0$ in the redshift range of interest here.

We are now able to assess how intergalactic absorption will modify the intrinsic photometric properties of galaxies at high redshift. At $z_{em} \sim 1.9$, Lyα line blanketing starts to cause an apparent depression of the U_n band continuum. As higher order lines of the Lyman series move into the bandpass, ΔU_n increases rapidly until, at $z_{em} = 3$, sources in the background appear, on average, ~ 1.5 mag fainter in the ultraviolet. By $z_{em} = 3.5$, Lyman-continuum absorption from forest clouds and Lyman limit systems is so severe, $\Delta U_n \sim 4.5$ mag (of which ~ 3 mag are due to Lyman-α clouds alone), that galaxies are effectively undetectable in this bandpass. Similarly, the Lyα line enters progressively the B band beyond $z_{em} \sim 2.5$. At $z_{em} = 3.3$, line blanketing from the Lyman series produces $\Delta B > 0.6$ mag. By $z_{em} = 3.7$, Lyman-continuum absorption contributes significantly to the total opacity, and the magnitude increment ΔB exceeds 1.4 mag.

Although Figure 4 refers to the average accumulated absorption only, rms fluctuations away from the mean values are predicted to be relatively modest, due to the broadband nature of the filters used (Press et al. 1993; Zuo 1993). For example, the B-band continuum of a galaxy at $z_{em} = 3.5$ is attenuated by the blanketing of, on average, more than 90 Lyα lines along the light travel path with $W > 0.3$ Å. Excursions away from the average curve will be the largest in the U_n passband, due to the contribution to the photoelectric opacity by the rarer Lyman limit systems. The probability of intersecting such thick clouds is significant. With $dN/dz = 0.92(1 + z)^{0.68}$ absorbers per unit redshift with $N_{H\,I} > 1.59 \times 10^{17}$ cm^{-2}, as many as $\Delta N \sim 1.4$ Lyman limit systems along a random path to $z_{em} = 3.5$ would be expected, on average, to photoelectrically absorb photons in the U_n band. The probability of intersecting at least one metal system, $P(\geq 1) = 1 - e^{-\Delta N}$, is then as large as $\sim 80\%$.

3.2. *The Colors of Primeval Galaxies*

It is of fundamental importance for our understanding of galaxy formation to know what the stellar radiation was like for young, primeval galaxies actively forming stars at high z. The observed colors of distant objects will be the sum of their intrinsic colors and the stochastic reddening they suffer along the path, and dereddening is only possible in a statistical sense. We illustrate few examples in detail. We compute the ultraviolet spectra for star-forming galaxies using the isochrone synthesis spectral evolutionary code of Bruzual & Charlot (1993). Nearly all the ionizing radiation from a stellar population is produced by massive stars on the main sequence. The models have solar metallicities and rely on Kurucz (1979) model atmospheres at far-UV wavelengths for stars in all stages with effective temperatures $40{,}000 < T_{eff} < 50{,}000$ K. The spectra of stars with higher T_{eff} (Wolf-Rayet stars and central stars of planetary nebulae) are approximated by unblanketed blackbodies.

We consider two extreme histories of star formation in the model galaxies: an instantaneous burst, appropriate, e.g., for star clusters that form on short timescales; and a constant star formation rate (SFR). Intermediate models characterized by exponentially declining SFR with timescale t_{burst} have the colors of a constant SFR model for $t < t_{burst}$, after which they resemble a single burst population (Bruzual & Charlot 1993). We assume a Salpeter initial mass function (IMF) with lower and upper cutoffs of 0.1 and 125 $M_\odot$ and ignore the effects of H I in the local interstellar medium on the transfer of ionizing photons.

Figure 5*a* depicts the spectral energy distribution of a stellar population at $z_{em} = 3.5$, with constant SFR at ages 0.05, 0.1, 0.3, and 0.6 Gyr, as observed at Earth. The unreddened rest-frame UV continuum is fairly flat except for a Lyman break at 912 Å and a Lyα narrow absorption feature from stellar photospheres and is nearly independent of age because of the continuous input of young massive stars. Ultraviolet synthetic spectra can be significantly bluer than this only if the stellar populations are younger than 10^7 yr or their IMF is unusually enriched with massive stars. The mean transmitted fluxes, as modified by intergalactic absorption along the path, are also plotted in the figure. For comparison, we have also filtered the 0.6 Gyr stellar spectrum through a dust extinction curve. We assume Galactic-type dust with $E_{B-V} = 0.05$ at the emission redshift, and find that this amount of dust absorption can mimic fairly well the effect of intergalactic attenuation in the wavelength range between rest-frame Lyα and the Lyman break. Figure 5*b* shows the observed spectral energy distribution of a stellar population at $z_{em} = 4$, for an instantaneous starburst at ages 0.01 and 0.05 Gyr. The UV light drops after 10^7 yr, when the most massive stars evolve off the main sequence.

Colors can be more readily interpreted using the AB-magnitude system

$$m_{AB} = -2.5 \log \int f_t(\nu) e^{-\tau_{eff}} T(\nu) d\nu - 48.59 , \qquad (20)$$

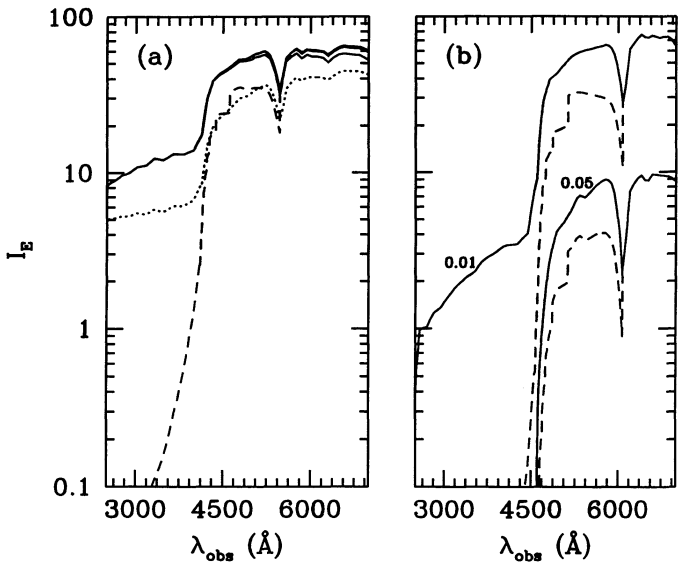

FIG. 5.—Spectral energy distribution of a stellar population at high redshift, as observed at Earth. Flux units are arbitrary. The rest-frame UV spectra are computed using Bruzual & Charlot's (1993) stellar population synthesis code. The models assume a Salpeter IMF with lower and upper cutoffs of 0.1 and 125 $M_\odot$. (*a*) $z_{em} = 3.5$, constant SFR at ages 0.05, 0.1, 0.3, and 0.6 Gyr. *Solid lines*: Unattenuated spectra. *Dotted line*: 0.6 Gyr stellar spectrum filtered through a Galactic dust extinction curve with $E_{B-V} = 0.05$ at the emission redshift. *Dashed line*: Mean transmitted flux, 0.6 Gyr no-dust case, as modified by intergalactic absorption. (*b*) $z_{em} = 4$, unattenuated instantaneous starburst (*solid lines*). The age in Gyr is indicated next to the spectra. *Dashed lines*: Same, as modified by intergalactic absorption.

where $f_t(\nu)e^{-\tau_{eff}}$ is the mean incident power measured in ergs cm^{-2} s^{-1} Hz^{-1}, and the subscript "t" denotes the flux which would be observed in the limit of negligible intergalactic absorption. We put our magnitudes directly into the *AB* system, so that $U_n = B = G = \mathcal{R}$ corresponds to a spectrum for which $f_t(\nu)e^{-\tau_{eff}}$ is constant.

Figure 6 displays the observed $U_n - B$, $B - \mathcal{R}$, and $G - \mathcal{R}$ colors versus emission redshift of our template attenuated galaxy for the no dust, constant SFR at age 0.6 Gyr case, together with the unobscured values. The intrinsic spectral shape has been kept constant with cosmic time. As expected, the observed colors redden quite sharply with redshift. At $z_{em} = 3$, the unobscured stellar spectrum, with $(B-\mathcal{R})_t \simeq 0.1$ mag, is reddened due to line blanketing to $B - \mathcal{R} \simeq 0.4$ mag. At $z_{em} = 3.5$, $(B-\mathcal{R})_t \simeq 0.6$ mag and $B - \mathcal{R} \simeq 1.3$ mag. By $z_{em} = 4$, $(B-\mathcal{R})_t \simeq 1.2$ mag, and Lyman-continuum absorption produces $B - \mathcal{R} \simeq 2.8$ mag. The observed $G - \mathcal{R}$ color behaves similarly, ranging from 0.2 mag at $z_{em} = 3$ to 1.7 mag at $z_{em} = 4$. For comparison, Galactic-type dust with $E_{B-V} = 0.05$ at the emission redshift would produce, in the interval $z_{em} = 3$–3.5, an extra $\sim$0.3 mag of reddening in both $B - \mathcal{R}$ and $G - \mathcal{R}$.

4. SUMMARY AND DISCUSSION

In this paper we have presented a detailed study of the reddening of background sources caused by Poisson-distributed foreground H I clouds. Much of the preceding material can be summarized as follows:

1. Through a standard curve-of-growth analysis, we have estimated the attenuation expected at wavelengths shortward of 1216 Å in the emitter rest-frame from the blanketing of lines in the Lyman series. In the redshift range $2.5 \lesssim z_{em} \lesssim 4.5$ of interest in this study, the blanketing opacity is dominated by the Lyman-α forest. Our simplified absorption model is consistent with the observed flux deficits D_A and D_B, and with the relative strengths of Lyβ, Lyγ, and Lyδ to Lyα absorption as recently measured by Press et al.

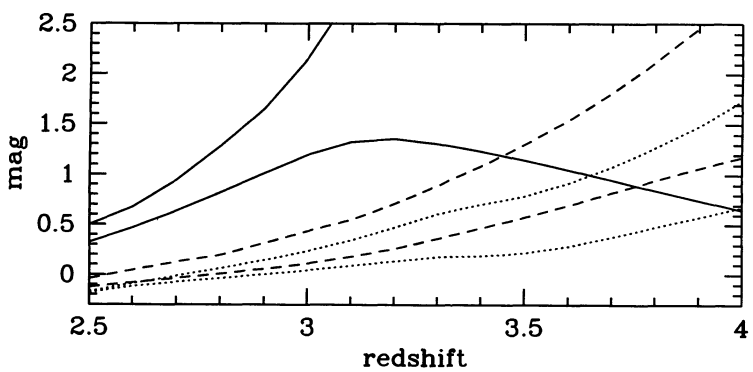

FIG. 6.—Apparent colors of a star-forming galaxy with constant SFR (age 0.6 Gyr, no dust), plotted as a function of the emission redshift. Each pair of curves depicts, from top to bottom, the attenuated colors and the colors observed in the case of negligible cosmological absorption. *Solid lines*: $U_n - B$. *Dashed lines*: $B - \mathcal{R}$. *Dotted lines*: $G - \mathcal{R}$. The intrinsic spectral shape has been kept constant with cosmic time.

(1993). The onset of line blanketing from the Lyman series with redshift is quite sudden, due to the rapid evolution of the forest clouds. A characteristic staircase profile is produced in the transmitted power.

2. Along with resonant line scattering, we include photoelectric absorption from neutral hydrogen in the Lyman-α clouds and Lyman limit systems along the line of sight. We adopt, as in previous studies, a power-law column density distribution with exponent 1.5 as $N_{\rm H\,I}$ varies from 10^{12} to 10^{20} cm^{-2}. It is fair to caution the reader, however, that the information on optically thin absorbers with $10^{16} \lesssim N_{\rm H\,I} \lesssim 10^{17}$ cm^{-2} is very limited. Clouds within this column density range dominate the contribution of the Lyman-α forest to the continuum cosmic opacity, which is therefore subject to large uncertainties.

3. We have studied the optical properties of high-z galaxies in four broad passbands, U_n, B, G, and $\mathscr{R}$. We find that, even if a young galaxy at $z_{\rm em} \lesssim 3$ radiated a significant amount of ionizing photons, the attenuation due to the accumulated photoelectric optical depth along the path produces a large reduction of the U_n band continuum. A discontinuity across the rest-frame Lyman limit of a galaxy is also characteristic of the integrated spectra stellar populations. A Bruzual model spectrum with Salpeter IMF and constant SFR has a 1.4 mag jump at 912 Å. While it is possible that nonstellar far-UV radiation, either from an AGN component or from supernova remnants (Shull & Silk 1979; Bithell 1991) may lead to a much smaller intrinsic Lyman break, we stress that the detection in the U_n band of a galaxy at $z_{\rm em} \gtrsim 3$ appears, in the presence of intergalactic attenuation, rather unlikely. This conclusion does not depend on the existence of any intrinsic absorption from the possibly gas-rich galaxy itself: we have assumed that all the stellar UV photons shortward of the Lyman limit will actually escape into intergalactic space.

4. Because of the stochastic attenuation suffered along the light travel path, galaxies at high redshift will be much redder in $B-\mathscr{R}$ than expected from a stellar population. Indeed, at $z_{\rm em} \sim 3.5$, the mean attenuation in the B band is ~ 1 mag. As an illustrative example, we have modeled the intrinsic UV photon distribution of star-forming galaxies with a stellar population synthesis code (Bruzual & Charlot 1993) and shown that the observed obscured colors of primeval galaxies redden quite sharply with redshift. The $B-\mathscr{R} \sim 0$ criterion for identifying flat-spectrum, star-forming galaxies is therefore biased against objects with $z_{\rm em} > 3$.

5. The Lyman decrement associated with the cumulative effect of absorbing material along the line of sight may provide a distinctive feature for identifying high-z galaxies. Deep multicolor continuum observations may be used to select those sources which are detected in the red but drop out of the bluer band image. This fact has been qualitatively exploited by Guhathakurta et al. (1990), who have argued that the lack of Lyman break objects down to $B \sim 27$ constrains the bulk of the faint, blue galaxy population to under $z_{\rm em} \sim 3$. Steidel & Hamilton's (1992, 1993) multicolor deep survey makes use of QSO absorption-line systems in the redshift range $3 \lesssim z_{\rm abs} \lesssim 3.5$ to locate high-z galaxy candidates. The broad ultraviolet passband is optimally placed below the Lyman edge of any galaxies associated with the optically thick absorption system, such that the bright QSO in the background is completely black, and the broadband colors of extremely faint objects near the QSO sightline can be obtained. Candidate primeval galaxies at the absorber's redshift are singled out by their faint apparent $\mathscr{R}$ magnitude, relatively flat $G-\mathscr{R}$ colors, and extremely red U_n-G colors.

Two objects in the extensively studied Q0000−263 field have been identified as $z_{\rm em} \sim 3.4$ radio-quiet galaxies. If their optical colors are typical of the galaxy population at that redshift, the two sources might be ideal candidates for a preliminary comparison of our model predictions with the observations. The two putative distant galaxies are undetected in the U_n bandpass and have similar G and $\mathscr{R}$ magnitudes and colors (Steidel & Hamilton 1993)

$$\text{Object A:} \quad \mathscr{R} = 24.8 \pm 0.3\,; \quad U_n - G > 1.9\,; \quad G-\mathscr{R} = 0.7 \pm 0.4\,,$$

$$\text{Object G2:} \quad \mathscr{R} = 24.2 \pm 0.1\,; \quad U_n - G > 1.7\,; \quad G-\mathscr{R} = 1 \pm 0.2\,.$$

Galaxy "G2" was discovered by Macchetto et al. (1992) on the basis of its strong Lyα emission (which affects only weakly its photometric properties in the given magnitude system), while galaxy "A" has been plausibly associated, by the proximity to the QSO line of sight, with a damped Lyman-α absorption system (Steidel & Hamilton 1992). According to our model of intergalactic absorption, detection in the U_n band is very unlikely at $z_{\rm em} \gtrsim 3$. Coupling a Bruzual stellar population spectrum for a constant SFR with our model for the continuum blanketing from the Lyman-α forest, we predict that young galaxies at this redshift will typically have $G-\mathscr{R} \sim 0.8$ mag. Our estimates place the two objects within the realm of what might be called "normal," flat-spectrum galaxies at redshift ~ 3.5, attenuated by intergalactic H I absorption. Dust extinction, if present, is likely to be quite small. It is important to note, however, that model predictions are quite sensitive to the unknown evolutionary state of the galaxy (i.e., its star formation history, whether it is undergoing a starburst, the duration of the starburst, the time elapsed since the starburst, etc.). While the differential reddening effects of QSO absorbers can be readily taken into account, our estimates for the colors of high-z galaxies are subject to substantial uncertainties.

It is now clear that blank-sky surveys for strong Lyα-emitting primeval galaxies are not particularly efficient. Although such a population may exist at some extreme redshift $z_{\rm em} \gtrsim 6$, the null results obtained so far (e.g., Pritchet & Hartwick 1990; Lowenthal et al. 1990; Djorgovski & Thompson 1992) imply that strong Lyα emission is not a common characteristic of galaxies at more modest redshift. The method of obtaining multicolor observations of the emitter's rest-frame UV stellar continuum might therefore offer a unique possibility to successfully detect high-z galaxies. As noted by Steidel & Hamilton, the main limitation of broadband photometry is that it separates an intrinsically flat-spectrum object from an intrinsically red one only within a small redshift range, $3 \lesssim z_{\rm em} \lesssim 3.5$. At $z_{\rm em} \gtrsim 3.5$, as line blanketing from intergalactic clouds significantly reddens the observed $G-\mathscr{R}$ (or, equivalently, $B-\mathscr{R}$) colors, a nondetection in the U_n bandpass is not an unambiguous indicator of a Lyman-continuum break anymore. Complementary intermediate-band imaging methods might, however, provide significative advantages. We suggest here to use, as tracers of redshift, the apparent discontinuities which will be present in the low-resolution spectra of background UV sources because of the blanketing by absorption lines in the Lyman series. Consider, for example, the apparent magnitude jump expected just shortward of Lyα in the emitter rest frame. At $z_{\rm em} = 3.5$ (4), galaxy spectra will typically have a drop of ~ 0.7 mag (1 mag) due to Lyα line blanketing. Two intermediate-band (FWHM $\sim$ 200 Å) filters, strategically placed to straddle this Lyα discontinuity, could

offer the necessary spectral resolution to probe the existence of sharp features in otherwise flat spectra, thereby providing a tool to identify high-z galaxies.

We have benefited from discussions with F. Haardt and C. Steidel. We thank S. Charlot for providing a copy of the stellar population synthesis code. This research was partially supported by NASA through grant GO4599.01-92A from the Space Telescope Science Institute, which is operated by the Association of Universities for Research in Astronomy, Inc., under contract NAS5-26555.

REFERENCES

Bechtold, J., Weymann, R. J., Lin, Z., & Malkan, M. 1987, ApJ, 315, 180
Bithell, M. 1991, MNRAS, 253, 320
Bruzual A., G., & Charlot, S. 1993, ApJ, 405, 538
Carswell, R. F., Lanzetta, K. M., Parnell, H. C., & Webb, J. K. 1991, ApJ, 371, 36
Chambers, K. C., Miley, G. K., & Van Breugel, W. J. M. 1990, ApJ, 363, 21
Cristiani, S., Giallongo, E., Buson, L. M., Gouiffes, C., & La Franca, F. 1993, A&A, 268, 86
Djorgovski, S., & Thompson, D. 1993, in IAU Symp. 149, The Stellar Populations in Galaxies, ed. A. Renzini & B. Barbuy (Dordrecht: Kluwer), 337
Giallongo, E., & Cristiani, S. 1990, MNRAS, 247, 696
Giallongo, E., & Trevese, D. 1990, ApJ, 353, 24
Guhathakurta, P., Tyson, J. A., & Majewski, S. R. 1990, ApJ, 357, L9
Fall, S. M., & Pei, Y. C. 1989, ApJ, 337, 7
———. 1993, ApJ, 402, 479
Kurucz, R. L. 1979, ApJS, 40, 1
Lilly, S. J., Cowie, L. L., & Gardner, J. P. 1991, ApJ, 369, 79
Lowenthal, J. D., Hogan, C. J., Green, R., Caulet, A., Woodgate, B., Brown, L., & Foltz, C. 1991, ApJ, 377, L73
Lowenthal, J. D., Hogan, C. J., Leach, R. W., Schmidt, G. D., & Foltz, C. 1990, ApJ, 357, 3
Macchetto, F. D., Lipari, S., Giavalisco, M., Turnshek, D. A., & Sparks, W. B. 1993, ApJ, 404, 511
Madau, P. 1991, ApJ, 376, L33
———. 1992, ApJ, 389, L1
Meiksin, A., & Madau, P. 1993, ApJ, 412, 34
Miralda-Escudé, J., & Ostriker, J. P. 1990, 350, 1
Møller, P., & Jakobsen, P. 1990, A&A, 228, 299
Murdoch, H. S., Hunstead, R. W., Pettini, M., & Blades, J. C. 1986, ApJ, 309, 19
Oke, J. B., & Korycansky, D. G. 1982, ApJ, 255, 11
Ostriker, J. P., & Heisler, J. 1984, ApJ, 278, 1
Paresce, F., McKee, C., & Bowyer, S. 1980, ApJ, 240, 387
Press, W. H., & Rybicki, G. B. 1993, ApJ, 418, 585
Press, W. H., Rybicki, G. B., & Schneider, D. P. 1993, ApJ, 414, 64
Pritchet, C. J., & Hartwick, F. D. A. 1990, ApJ, 355, L11
Rauch, M., Carswell, R. F., Chaffee, F. H., Foltz, C. B., Webb, J. K., Weymann, R. J., Bechtold, J., & Green, R. F. 1992, ApJ, 390, 387
Sargent, W. L. W., Boksenberg, A., & Steidel, C. C. 1988, ApJS, 68, 539
Sargent, W. L. W., Steidel, C. C., & Boksenberg, A. 1989, ApJS, 69, 703
Schneider, D. P., Schmidt, M., & Gunn, J. E. 1991a, AJ, 101, 2004
———. 1991b, AJ, 102, 837
Shull, J. M., & Silk, J. 1979, ApJ, 234, 427
Steidel, C. C. 1990, ApJS, 74, 37
Steidel, C. C., & Hamilton, D. 1992, AJ, 104, 941
———. 1993, AJ, 105, 2017
Steidel, C. C., & Sargent, W. L. W. 1987, ApJ, 313, 171
Tyson, J. A. 1988, AJ, 96, 1
Tytler, D. 1987, ApJ, 321, 49
Wright, E. L. 1986, ApJ, 311, 156
Zuo, L. 1993, A&A, 278, 343
Zuo, L., & Phinney, E. S. 1993, ApJ, 418, 28